JACS
JOURNAL OF THE AMERICAN CHEMICAL SOCIETY
Article
pubs.acs.org/JACS

Design Rules for Organic Donor–Acceptor Heterojunctions: Pathway for Charge Splitting and Detrapping

Carl Poelking*[,†,‡] and Denis Andrienko*[,†]

[†]Max Planck Institute for Polymer Research, Ackermannweg 10, 55128 Mainz, Germany
[‡]Heidelberg Graduate School of Fundamental Physics, INF 226, 69120 Heidelberg, Germany

ABSTRACT: Organic solar cells rely on the conversion of a Frenkel exciton into free charges via a charge-transfer state formed on a molecular donor–acceptor pair. These charge-transfer states are strongly bound by Coulomb interactions and yet efficiently converted into charge-separated states. A microscopic understanding of this process, though crucial to the functionality of any solar cell, has not yet been achieved. Here we show how long-range molecular order and interfacial mixing generate homogeneous electrostatic forces that can drive charge separation and prevent minority carrier trapping across a donor–acceptor interphase. Comparing a variety of small-molecule donor-fullerene combinations, we illustrate how tuning of molecular orientation and interfacial mixing leads to a trade-off between photovoltaic gap and charge-splitting and detrapping forces, with consequences for the design of efficient photovoltaic devices.

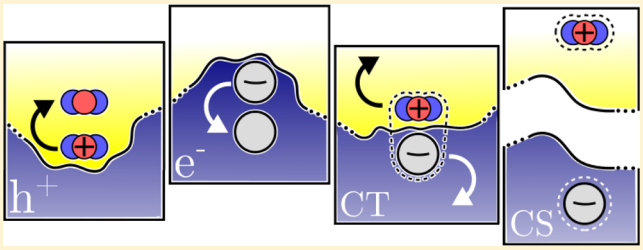

1. INTRODUCTION

The efficiency of organic solar cells can be expressed as the product of the open-circuit voltage (V_{oc}), short-circuit current (J_{sc}), and fill factor (FF). These quantities have complex interdependencies, as they derive from just a few elementary processes. Mechanisms that enhance J_{sc}, for example, connect with strong absorption, high charge-carrier mobilities, and efficient charge extraction. Building on the success of the bulk heterojunction concept, strategies in pursuit of higher short-circuit currents therefore employ light-absorbing nonfullerene acceptors,[1,2] low-band gap polymers,[3] materials for singlet-exciton fission,[4,5] or triple-layer energy-relay cascade structures[6] as building blocks.

Recipes that target V_{oc} involve either morphological tuning,[7,8] insertion of interlayers[9] or manipulations of the chemical structures of the active materials.[10] Furthermore, in an attempt to prescreen suitable donor–acceptor combinations, a correlation of V_{oc} with the sum of the gas-phase ionization energy (IE_0) of the donor and electron affinity (EA_0) of the acceptor is typically assumed. However, such a correlation is coincidental rather than systematic, as it neglects the impact of molecular fields that in turn depend on the molecular packing and orientation in the solid state.

A rigorous evaluation of the thermally broadened density of states (DOS) of donor and acceptor species, by contrast, shows that calculation of the charge-density-dependent (as opposed to illumination-intensity-dependent) V_{oc} is possible.[11] Regrettably, such an approach can still be misleading, as it imposes a finite steady-state charge density and hence does not verify whether charges are generated in the first place. For illustration, consider the level schematics presented in Figure 1a,b: both pertain to the interface between C_{60} and the merocyanine dye EL86, in its tip-on (Figure 1a) and face-on (Figure 1b) orientations. With sizable level offsets, comparable E_{ct} and a gas-phase Frenkel exciton energy of 2.8 eV, both configurations (a) and (b) appear suitable for a solar cell. Using correlations established between photovoltaic gap Γ, charge-transfer (CT) state energy, and V_{oc}, the face-on configuration is hence expected to yield an open-circuit voltage that is roughly 0.6 eV larger than in the tip-on scenario. And yet, we will rationalize in this work why the

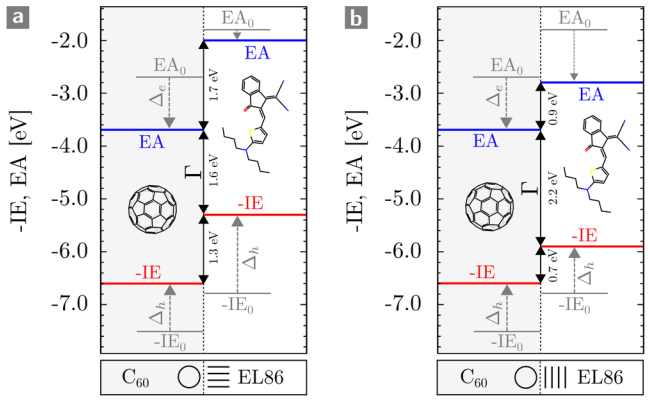

Figure 1. Level schematics for C_{60}/EL86. (a) Tip-on orientation of EL86 on C_{60} with a small photovoltaic gap Γ versus the (b) face-on orientation with large Γ. Gas-phase ionization energies and electron affinities are denoted as IE_0 and EA_0, respectively. Δ_e (Δ_h) are the intermolecular electrostatic and polarization contributions to electron (hole) energies.

Received: February 27, 2015
Published: April 22, 2015

DOI: 10.1021/jacs.5b02130
J. Am. Chem. Soc. 2015, 137, 6320–6326

face-on scenario does not yield an efficient (i.e., charge-generating) interface at all.

More generally, we will address three questions. First, what is the maximum V_{oc} that can be harvested from a given donor−acceptor pair? Second, which interfacial morphology is required to retain a functional device? Third, how can CT states split up quickly and efficiently? All three questions are ultimately linked to the (controversial) energetics of CT and charge-separated (CS) states at donor−acceptor heterojunctions: As an example, the CT-binding energy (E_{ct}) calculated for ideal interfaces is still of the order of 0.3 eV, even in high-performing systems such as the 8.3% efficient oligothiophene derivative DCV5T-Me(3,3) (D5M) combined with C_{60}.[12,13]

With E_{ct} approximately 10 times larger than the room-temperature k_BT, fast and efficient charge separation appears unlikely. Charge delocalization, though helpful, would draw fewer benefits from dielectric solvation and not necessarily neutralize the Coulomb attraction in such a way that charges separate without the need for thermal activation,[14,15] in particular in small-molecule-based solar cells with strong dyes. Similar reasoning applies to entropy-driven separation[16] or long-range charge transfer,[17] neither of which boost rates to an extent that justifies an ultrafast process. Continuous level bending has been proposed as a further pathway for cold-exciton breakup,[18] but it would still lead to locally bound CT states, and, more importantly, will not hold in the presence of mesoscale order, which yields flat level profiles.[11]

Unveiling possible pathways for charge separation, which is still a microscopically poorly understood process,[14−17,19−22] is one of the targets of this paper. In particular, we show how the energy landscape that emerges from mesoscale order provides push-out forces that can drive the charge separation process; in line with the apparent absence of a Coulomb barrier claimed for some systems.[15] In deriving the functional difference between chemically versus electrostatically generated level offsets, we rationalize why donor−acceptor intermixing can be beneficial for a functioning device and identify trade-offs and structure−energy relationships to be considered in the design of solar-cell devices.

2. METHODS

We will here describe the computational procedure followed in this work. To compute the energetics of molecular excitations (here: charges and CT states), we employ a perturbative description built on a classical expansion of molecular fields in terms of distributed atomic multipoles and polarizabilities, parametrized from first-principles calculations.[23−26] Starting from gas-phase energetics, we hence compute the electrostatic ($W^{(1)}$) and polarization ($W^{(2)}$) contribution $W = W^{(1)} + W^{(2)}$ to the energies of molecular excitations embedded in the organic solid, simulated with atomistic resolution.[27] The relevant contributions to ionization energies (IEs) and electron affinities (EAs), for example, are then given by the energy differences $\Delta_h = W_h - W_n$ and $\Delta_e = W_e - W_n$, respectively, where subscripts n (neutral), h (hole), and e (electron) specify the charge state. This and comparable perturbative approaches have been applied to disordered[28,29] and ordered[13,18,30−33] organic semiconductors, in bulk and at interfaces.

All energy calculations in this work are carried out using the embedding procedure implemented in the VOTCA package.[11,28] As an essential feature of this approach, we explicitly account for all long-range electrostatic interactions to which the excitations are subjected. Such an extension is necessary, as the interaction sum associated with a net charge embedded in a net-quadrupolar environment is in general only conditionally convergent.[11,34] Inclusion of appropriate shape terms lifts the apparent degeneracy between thin-film and bulk levels for molecular ions. The $1/r^3$ character of the charge−quadrupole interaction nevertheless results in a rather slow convergence for a thin-film setup, with the effect that the energetics is tied to the degree of mesoscale order.

For the purpose of this work, we stress that the long-range treatment of the quadrupolar background generates an abrupt step in the electrostatic potential across the donor−acceptor interface, as opposed to continuous electrostatic profiles that result from any short-range description. This electrostatically generated offset can either amplify or reduce the offset between the gas-phase IEs and EAs of the donor and acceptor. Approaching the thin-film case, level bending at the interface typically disappears, resulting in flat level profiles. It has been shown that this thin-film scenario with at least uniaxial, preferential alignment of molecules on a mesoscale provides exceptional agreement between calculated and measured energy levels.[11]

3. CHARGE SPLITTING FORCES

To understand how electrostatics can promote barrier-less CT separation through the action of long-range electrostatic fields, we consider a donor−acceptor interphase, that is, an interfacial region characterized by intermixing of the donor and acceptor molecular species. Absent at sharp (i.e., flat) heterojunctions, this type of interphase has been found to improve exciton yield in polymer−fullerene devices.[35,36] We expand on this observation and study, as a proof of concept, small protrusions of C_{60} into a D5M domain. The atomistic model, equilibrated via molecular dynamics, consists of a C_{60} substrate and D5M film, each of 10 nm thickness. The total interfacial area amounts to 40 nm^2. The protrusion takes up approximately 10% of this area.

Simulation results for the atom-resolved environment contribution Δ_e to electron affinities are shown in Figure 2a. In the projection of the energy landscape of the fullerene region, averaging is performed over a 2 nm slice that fully incorporates the C_{60} appendix. Notably, the abrupt step in Δ_e across the interface, which results from the coherent action of quadrupolar fields of the D5M, persists, as these fields are generated nonlocally, i.e., they are the combined effect of millions of preferentially oriented molecules that together define the electrostatic surrounding on a mesoscale.[37] Figure 2a therefore shows that the electron states on minority acceptor molecules (those molecules that form part of the protrusion) adopt the electrostatic character of the majority donor domain: They are acceptor states with a donor electrostatic dressing and as such experience a reduced stabilization. The reduction amounts to around 0.2 eV: This almost matches the total CT binding energy for this system. The total binding energy, however, consists of multiple smaller contributions, which are associated with individual hopping events that, executed in succession, transform a CT into a CS state, in other words, the competition between Coulomb attraction and dielectric solvation locally leads to smaller barriers for separation. The largest of these local hopping barriers occur during the conversion from a nearest-neighbor electron−hole pair to a next-nearest and next-next-nearest-neighbor pair. Specifically, the first two hopping barriers together amount to only 0.2 eV. The 0.2 eV can be harvested for these first two and most crucial steps in the separation process, which as a result is locally driven.

In spite of its model character, this analysis already shows that mesoscale fields can be used to generate a stepped energy cascade that locally drives the charge splitting process.[38] The cascade is in this case an intrinsic property, rather than the result of a tailored interlayer comprising a third molecular

DOI: 10.1021/jacs.5b02130
J. Am. Chem. Soc. 2015, 137, 6320−6326

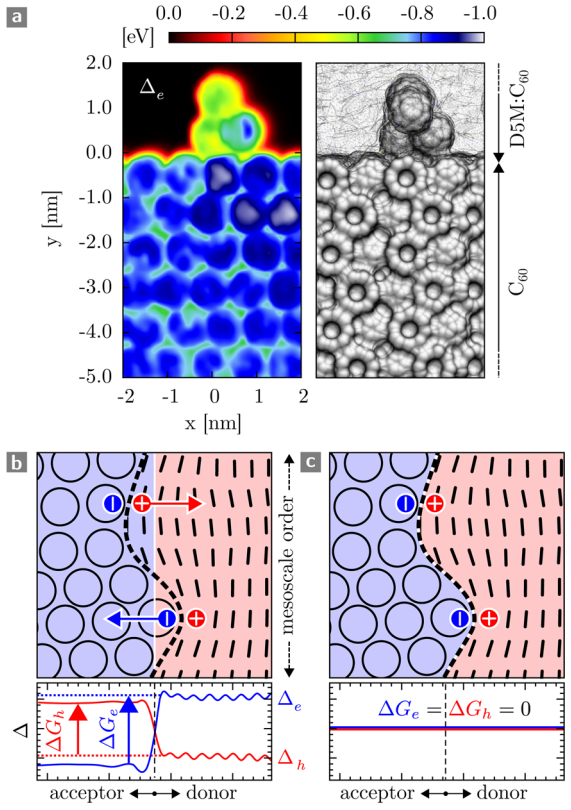

Figure 2. Charge push-out in C_{60}/D5M. (a) Color map of the projected electrostatic and polarization contribution Δ_e to electron affinities. The atomistic morphology accommodates a small fullerene protrusion into the D5M donor domain. This protrusion is subjected to mesoscale fields generated within the donor majority domain. The resulting driving force for charge push-out ΔG_e functionally distinguishes an electrostatically (b) from a chemically (c) generated level offset.

species.[6,39] The homogeneity of the mesoscale fields also implies an important functional difference between an electrostatic and a purely chemical level offset, pointed to in Figure 2b,c: Only the electrostatic offset (Figure 2b) provides driving forces ΔG for minority electron and hole push-out:

$$\Delta G_e = \Delta_{e(A)}|_D - \Delta_{e(A)}|_A$$
$$\Delta G_h = \Delta_{h(D)}|_A - \Delta_{h(D)}|_D \quad (1)$$

Here, $\Delta_{e(A)}|_D$ denotes the environment contribution to the electron (e) state energy of the acceptor (A) embedded in the donor (D) domain. Definitions of the other Δ's follow by analogy. If donor and acceptor are electrostatically identical, $\Delta G_e = \Delta G_h = 0$; the total level offsets are then given simply by the respective chemical offsets, i.e., the difference in gas-phase IEs and EAs. Such a chemical offset (Figure 2c) may assist in generating CT states, but it cannot drive the CT separation process.

Comparing the cartoon from Figure 2b to the atomistic model from Figure 2a, we note that the atomistic morphology suffers from an important shortcoming: Only a tiny fraction of donor–acceptor pairs, specifically those pairs whose acceptor unit forms part of the small fullerene appendix, makes use of the push-out forces defined above. The large majority of interfacial electron–hole pairs, however, will be subjected to the full Coulomb barrier, and charge separation has to occur without the assistance of mesoscale fields. This picture is very different from the (at this point still purely conceptual) schematic in Figure 2b, where indeed hole–electron pairs over the entire interfacial area benefit from these driving forces.

A realistic model system should hence account for both donor–acceptor interpenetration on a domain scale and intermixing on a molecular scale. This is rather tricky to achieve on an atomistic level, as simulations would not only have to address very large system sizes,[40] but also appropriately sample the free energy landscape. We therefore switch to a lattice model, where each lattice site represents either a donor or acceptor molecule. For parametrization, reference molecules (here D5M and C_{60}) are electrostatically coarse-grained into multipolar polarizable lattice sites. To arrive at a more generic model, the multipole expansion of the D5M lattice site is furthermore reduced to the quadrupolar moment Q_{20} associated with the long molecular axis. Note that as the lattice model preserves the molecular quadrupole moment per volume, long-range interactions can be quantitatively accounted for.

The cubic lattice incorporates 8000 molecular sites spaced with a lattice constant of 0.55 nm. Metropolis Monte Carlo sampling is used to equilibrate the interfacial morphology, starting from a clean interface with the acceptor (donor) domain located in the halfspace $z < 0$ ($z > 0$) and the particle type of the bottom-most and top-most layers constrained. Pairwise nearest-neighbor interaction energies for donor–donor (ε_{DD}), donor–acceptor (ε_{DA}), and acceptor-acceptor (ε_{AA}) contacts were chosen as $\varepsilon_{AA} = \varepsilon_{DD}$ and $\varepsilon_{DA} - \varepsilon_{DD} = k_B T$. With these interaction parameters, the interphase between donor and acceptor comprises approximately two monolayers of composition 30%D:70%A and 70%D:30%A. The morphology is characterized by domain interpenetration rather than fine intermixing, as indicated by composition maps of the four monolayers closest to the interface, shown in Figure 3. The phenomenological contact interactions lead to an overall concentration profile shown in Figure 4c.

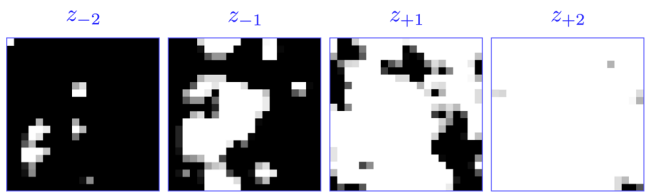

Figure 3. Interfacial morphology cross sections through a lattice interphase at $z_{-2} = -0.8$ nm (left) to $z_{+2} = +0.8$ nm (right). Acceptor (donor) regions are colored black (white). At z_{-1} and z_{+1}, the donor/acceptor ratio is 30%:70% and 70%:30%, respectively.

To assess the contribution of mesoscale fields to the charge separation process, we define charge push-out fields $f_{h(D)}(i,j)$ for hole transfer between nearest-neighbor donor sites i and j, and $f_{e(A)}(i,j)$ for electron transfer between nearest-neighbor acceptor sites:

$$f_{h(D)}(i,j) = \frac{\Delta_{h(D)}(j) - \Delta_{h(D)}(i)}{q(z_j - z_i)}$$
$$f_{e(A)}(i,j) = \frac{\Delta_{e(A)}(j) - \Delta_{e(A)}(i)}{q(z_j - z_i)} \quad (2)$$

DOI: 10.1021/jacs.5b02130
J. Am. Chem. Soc. 2015, 137, 6320–6326

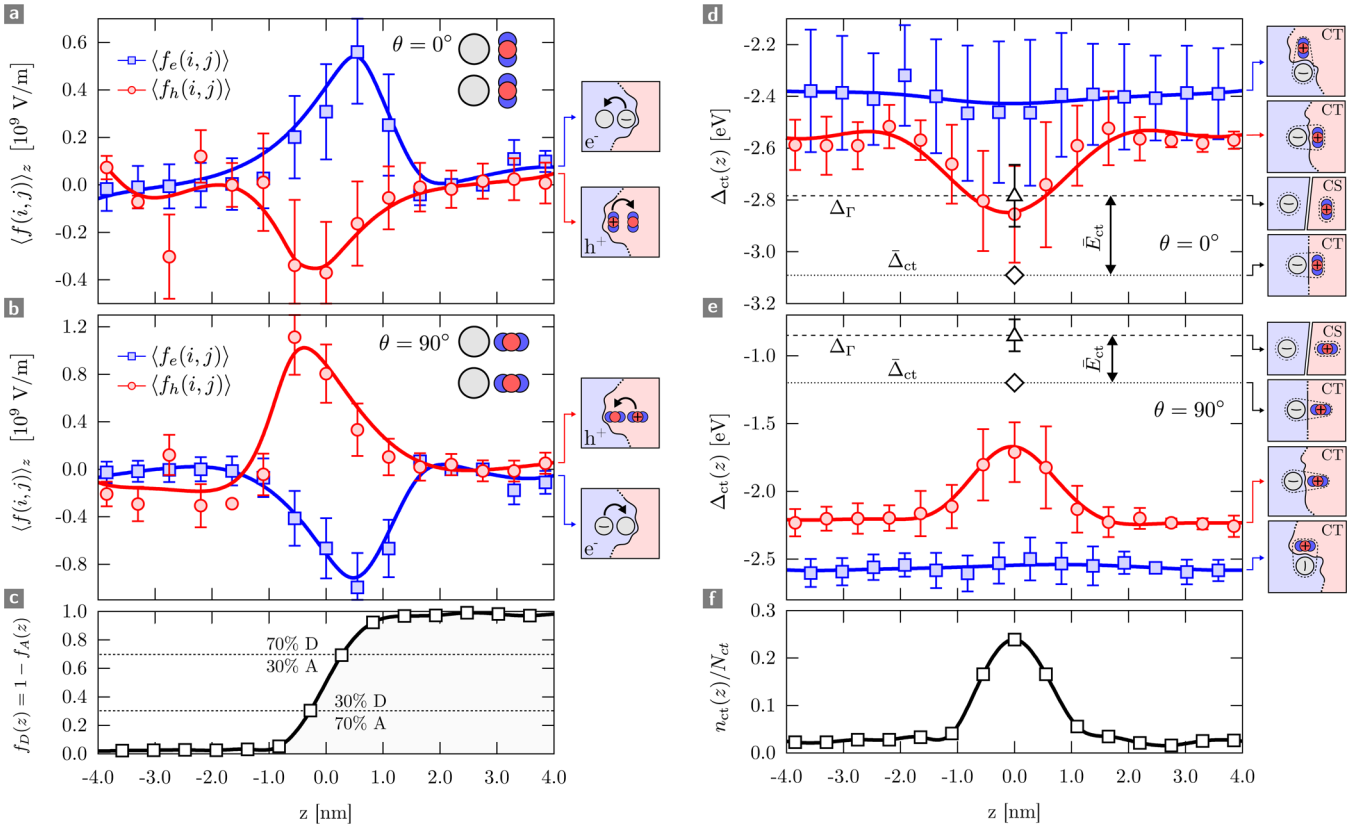

Figure 4. Charge push-out across a donor−acceptor interphase via mesoscale fields. Interfacial layer-averaged fields $\langle f_{h(D)}(i,j)\rangle_z$ and $\langle f_{e(A)}(i,j)\rangle_z$ (for definition, see text) across a heterojunction between quadrupolar polarizable donor sites and apolar polarizable acceptor sites in an (a) face-on and (b) tip-on orientation. The donor sites mimic an ADA-type compound with long-axis quadrupole moment $Q_{20} < 0$. The push-out fields are narrowly peaked over an interfacial region with the donor concentration profile given in (c). Polarity and magnitude of these fields impact the energetics of CT states as again illustrated for the (d) face-on and (e) tip-on case, where Δ_{ct} (electrostatic and polarization contribution to CT-state energies) is shown for pairs formed between adjacent layers (red line with circles) and within the same layer (blue line with squares). The resulting Δ_{ct} should be compared to the case of a sharp interface ($\bar{\Delta}_{ct}$, dotted line with diamond) as well as to the correction to the photovoltaic gap Δ_Γ. With most pairs found in the interphase region, as indicated by the pair concentration profile (f), mesoscale fields shift the CT-state energy for the face-on scenario into the photovoltaic gap, leading to unbound CT states. CT states in the tip-on scenario (e) experience the opposite effect: Δ_{ct} moves further away from Δ_Γ, leading to higher CT binding energies.

The z_i and z_j are the respective positions of sites i and j along the interface normal. A positive f implies a driving force directed toward the acceptor domain, irrespective of the sign of the charge $q = \pm 1$ e. The gross driving force from eq 1 can be formally recovered by integration over the layer-averaged pairwise driving fields $\langle f_{h(D)}(i,j)\rangle_z$ and $\langle f_{e(A)}(i,j)\rangle_z$, for example, $\Delta G_{h(D)} = -q\int\langle f_{h(D)}(i,j)\rangle_z dz$. These layer-averaged fields are plotted in Figure 4a,b as a function of the position along the interface normal. They have been calculated for two different molecular orientations of the donor site, face-on (Figure 4a) and tip-on (Figure 4b). Only the face-on configuration, however, yields the correct polarity of the interphase driving fields, pushing holes toward the donor and electrons toward the acceptor. In the tip-on orientation, the polarity is reversed: Trapping of charge carriers on minority sites is in this case probable. A solar cell built around the tip-on orientation is hence expected to suffer from trap-assisted recombination; here recombination of a majority carrier with a trapped minority carrier.

We now investigate how the push-out fields impact the energy landscape for CT states.[41] For reference, we first consider a flat interface, with all donor sites located in $z > 0$, acceptor sites in $z < 0$. We denote the electrostatic and induction contributions to the CT-state energy as $\bar{\Delta}_{ct}$ and the corresponding photovoltaic gap as $\bar{\Delta}_\Gamma$, where the bar indicates the flat interface. Both $\bar{\Delta}_\Gamma$ (dashed line with triangle) and $\bar{\Delta}_{ct}$ (dotted line with diamond) are shown in Figure 4d,e for the face-on (d) and tip-on (e) molecular orientations. In both cases, the CT binding energy, $\bar{E}_{ct} = \bar{\Delta}_\Gamma - \bar{\Delta}_{ct}$, amounts to the usual 0.3 eV.

For the system with finite interface roughness, the concentration profile of molecular pairs forming CT states is shown in Figure 4f. First, we note that this roughness, which leads to a broadened peak in the concentration profile, leaves the solid-state contribution to the photovoltaic gap unaffected, $\Delta_\Gamma = \bar{\Delta}_\Gamma = \Delta_{e(A)}|_A + \Delta_{e(D)}|_D$, as Γ only probes states located well within the donor and acceptor films. Δ_{ct}, however, proves rather sensitive to the degree of intermixing. Here, we distinguish between two types of CT states, either formed between two adjacent layers (red line with circles) or within the same layer (blue line with squares), as depicted on the right-hand side of Figure 4d,e. For the face-on configuration (Figure 4d), energies of CT states formed between two adjacent layers are shifted up by 0.3−0.5 eV compared to $\bar{\Delta}_{ct}$, even surpassing Δ_Γ away from the interface ($|z| \geq 0.6$), leading to a negative E_{ct}, and hence unbound CT states.

One should of course consider that CT states far away from the interface are absent for flat and rare for rough interfaces,

DOI: 10.1021/jacs.5b02130
J. Am. Chem. Soc. 2015, 137, 6320−6326

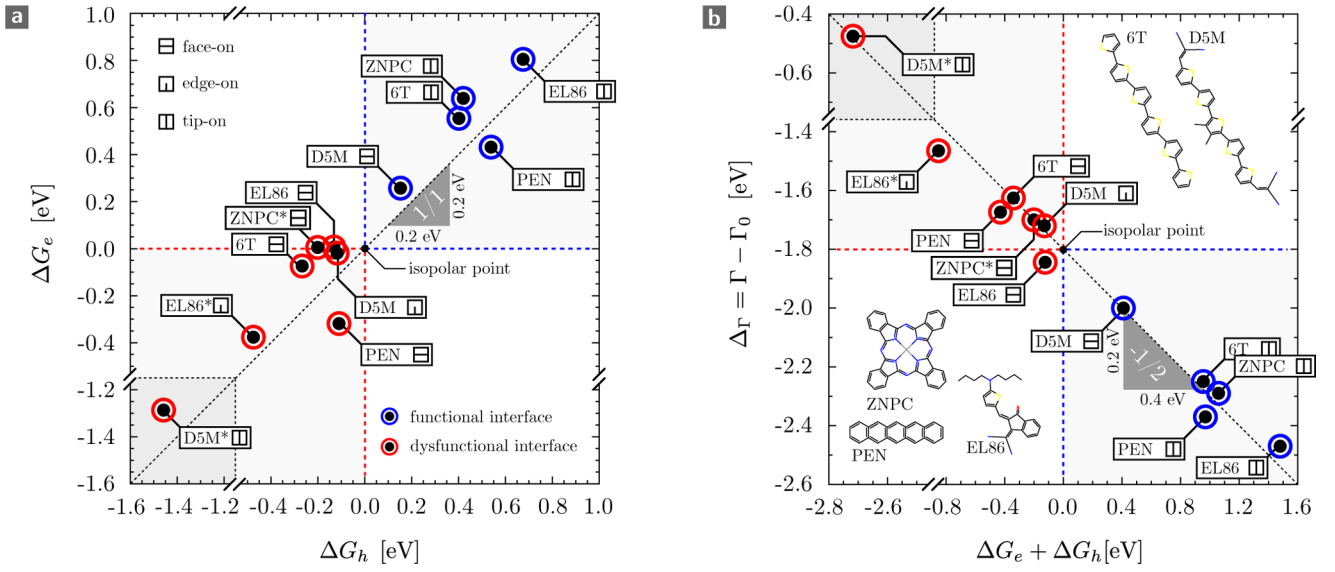

Figure 5. Trade-off between charge push-out and photovoltaic gap. (a) Correlation plot of driving forces ΔG_h and ΔG_h computed for five donor materials in combination with C_{60}, incorporating up to three interfacial orientations (face-on, tip-on, edge-on). Configurations found experimentally for the respective planar heterojunction are circled in blue. Configurations circled in red are expected to yield dysfunctional cells. (b) Trade-off between change in photovoltaic gap $\Delta_\Gamma = \Gamma - \Gamma_0$ versus total charge push-out force $\Delta G_h + \Delta G_e$. Calculations are performed on 10 nm donor films on top of 10 nm C_{60} or (for compounds marked with an asterisk) 10 nm dielectric with $\varepsilon \simeq 4$, shown to yield transferable results.

with the vast majority of the CT states found across a narrow interphase between $z = -1$ nm and $z = +1$ nm (see the pair concentration profile in Figure 4f). Across this interphase, charge push-out fields are particularly strong, and yet, Δ_{ct} in fact experiences a dip at around $z = 0$, as the high-energy minority hole and low-energy majority electron states in the acceptor domain ($z < 0$) are traded for high-energy minority electron and low-energy majority hole states in the donor domain ($z > 0$). Still, the mean binding energy in the $z = 0$ slice is only on the order of 0.05 eV, which should be thermally accessible.

The second type of CT state, with both charges located within the same layer, is subjected to an even larger total push-out force, such that the dip at $z = 0$ disappears (blue line in Figure 4d). At the same time, these CT states are shifted upward by an additional 0.2 eV due the anisotropy of the quadrupolar molecular species.[42]

For the alignment of the negative quadrupole component with the interface normal (Figure 4e), the scenario is reversed, as expected due to the opposite (and unfavorable) polarity of the push-out forces. Indeed, the CT binding energy is now increased by 0.3−1.0 eV. Depending on the internal energy landscape, CT states will then either dissociate in the wrong direction (effectively reversing the role of donor and acceptor) or simply remain stationary, until recombination occurs.

As a conclusion of the above, suitably tailored interfacial push-out forces can indeed shift CT-state energies into the photovoltaic gap, leading to unbound states. Correct polarity and magnitude of the forces depend on both molecular orientation and intermixing, with the latter giving rise to nanoscale surface roughness. So what happens upon varying the degree of this roughness? First off, for a fixed interfacial orientation, the gross driving forces ΔG_e(A) and ΔG_h(D) do not change with the degree of donor−acceptor intermixing. Consequently, as the size of the interphase grows, the area below the curves in Figure 2 is conserved, whereas the peak heights decrease, and the peak widths increase. This implies a trade-off between interphase size and magnitude of the charge push-out fields: If the interphase is too narrow, we have a scenario as seen for the atomistic D5M:C_{60} model, where pair splitting fields are sizable, but the fraction of interfacial sites that can harvest these fields is small. If the interphase is wide, the fraction of interfacial sites that are subjected to the pair splitting fields will be considerable, but the fields themselves may be insufficient to overcome E_{ct}. For a given donor−acceptor combination, the optimum degree of intermixing will hence depend on the relative magnitudes of E_{ct} on the one hand and ΔG_e and ΔG_h on the other hand.

4. DESIGN RULES

We have by now established that mesoscale order generates homogeneous, orientation-dependent charge push-out fields across a donor−acceptor interphase. The upper bound of these fields is set by the driving forces $\Delta G_{e(A)}$ and $\Delta G_{h(D)}$ that result from the difference in electrostatic and polarization contributions to site energies in the pristine donor and acceptor films. Poled correctly, they locally drive the charge separation process, provided they surpass the local Coulomb barriers that sum up to the total CT binding energy $\bar{E}_{ct}$ defined in the absence of any charge push-out fields. This binding energy is reasonably constant across different donor−acceptor materials, as a consequence of the similar dielectric properties that through dielectric solvation place $\bar{E}_{ct}$ around 0.3 eV.

The question arises: Which magnitudes of $\Delta G_{e(A)}$ and $\Delta G_{h(D)}$ are physically realizable (and realized) in organic solar cells to oppose this nevertheless strong attraction of the electron−hole pair, in particular in small-molecule-based systems? To address this, we have investigated five different donor materials used in combination with C_{60} as acceptor: pentacene (PEN), sexithiophene (6T), zinc-phthalocyanine (ZNPC), the merocyanine dye EL86 and acceptor-substituted oligothiophene D5M. Model interfaces were assembled from the crystal structures of the respective components: The C_{60} exposes its fcc [111] surface to the donor, whose X-ray crystal structures we cleaved to obtain the desired orientation on the

DOI: 10.1021/jacs.5b02130
J. Am. Chem. Soc. 2015, 137, 6320−6326

C_{60} substrate. The mismatch between the crystal faces was corrected by equilibration of the C_{60} using molecular dynamics.

Due to the orientation dependence, clearly no unique value for ΔG can be assigned to any given donor−acceptor combination. We have therefore incorporated up to three packing modes per donor, corresponding to face-on, edge-on, and tip-on molecular orientations. A summary of the computed charge push-out forces is provided in Figure 5a, which illustrates the expected linear correlation between ΔG_h and ΔG_e. The variation of the ΔG's with orientation can easily exceed 1 eV, as is observed for the strongly polar donor−acceptor- and acceptor−donor−acceptor-type materials EL86 and D5M, respectively. Strikingly, the experimentally reported configurations in the respective planar heterojunction solar cell are all located in the first quadrant, where ΔG_e, $\Delta G_h > 0$; this condition appears to be a prerequisite for functional solar cells. As has already been discussed in the context of the lattice model (Figure 4), there is a clear rationale why cells with negative charge push-out forces should suffer from inefficient charge generation and extraction: With ΔG_e, $\Delta G_h < 0$, charges are pushed out from the interphase in the wrong direction and hence trapped on minority sites. Correctly poled, the mesoscale fields therefore come with a dual benefit: they assist both charge splitting and minority-carrier detrapping. Of these two effects, the former is complementary, the latter essential. Indeed, relating back to Figure 1, the need for minority-carrier detrapping (and extraction) finally explains why only the tip-on configuration of EL86 on C_{60} is expected to work well without suffering from extensive recombination across the entire donor−acceptor interface.

The isopolar point, defined by $\Delta G_e = \Delta G_h = 0$, hence marks the border point between a dysfunctional and functional interface. This said, large positive ΔG's appear most desirable, but they come at the cost of a reduced photovoltaic gap (which linearly correlates with the CT-state energy and hence V_{oc}): To illustrate this, Figure 5b correlates the sum of ΔG_e and ΔG_h against the difference $\Delta_\Gamma = \Gamma - \Gamma_0$ in the photovoltaic gap evaluated in gas-phase (Γ_0) and in the solid state (Γ). The trade-off between Δ_Γ versus $\Delta G_e + \Delta G_h$ occurs at a rate of −1/2, since the acceptor IE and donor EA can be modified without impacting Γ. The largest reduction in Γ follows for the solar-cell configuration of EL86, in line with a sizable total push-out force of almost 1.5 eV. A push-out force on the order of the CT binding energy should, however, suffice to efficiently generate free charges. With the CT binding energy located at 0.3 eV, much of the 1.5 eV are hence wasted, even though a driving force of this magnitude may still be necessary in the case of strong donor−acceptor intermixing (as explained in Section 3). Otherwise they result in uncalled-for structural V_{oc} losses. Assuming perfect morphological control, a compromise between Γ and charge push-out forces is therefore obtained for operation just above the isopolar point marked in Figure 5a. It has in fact been realized for the face-on configuration of D5M, which balances driving forces for charge push-out and detrapping with moderate gap-related V_{oc} losses. This loss Δ_Γ (associated with the position of the mean of the DOS) is furthermore accompanied by a disorder-related impact on V_{oc} (associated with the tail of the DOS). D5M, for example, achieves an exemplary compromise for the former but performs rather poorly regarding the latter, due to sizable energetic disorder of 0.1 eV, the largest among all compounds studied here.

Last, but not least, the trade-offs identified above also hold for nonfullerene systems: A polar acceptor unit would, however, impose stricter orientational constraints, as an unfavorable acceptor orientation could then pin the interface to a negative ΔG whatever the orientation of the donor and vice versa. Independently of the type of acceptor used, molecular orientations with a negative ΔG and as a result enlarged Γ may also prevent Frenkel to CT exciton conversion; another reason why solar cells working in that regime may have deficiencies. In a similar way, the need to generate CT states from Frenkel excitons sets an upper limit for how much the CT-state energy may be raised through intermixing in configurations with $\Delta G > 0$.

5. CONCLUSIONS

We have demonstrated that mesoscale fields provide charge push-out and detrapping forces that can assist in the initial phase of electron−hole pair separation. These driving forces result from the coherent superposition of quadrupolar fields that accompany long-range molecular ordering in a thin-film setup. Due to their mesoscopic origin, they are characterized by pronounced in-plane homogeneity and an out-of-plane discontinuity. In the presence of mild donor−acceptor intermixing, they are sharply peaked over a narrow interphase and locally drive the charge-separation process if dimensioned sufficiently and poled correctly, pointing to the functional difference between chemically and electrostatically generated level offsets.

Correct polarity of the driving forces serves as a prerequisite for efficient solar-cell operation, as is suggested by the comparison of different donor materials and interfacial configurations. This observation indicates that the action of homogeneous push-out forces accounts for a pathway for charge separation that could not be realized with only charge delocalization[43] or energetic disorder.[21] The presence of these fields rationalizes why cold excitons[14] can suffice to obtain free charges and, most importantly, why separation can be barrierless.[15] If, however, they only barely compensate the exciton binding energy, then hot states[20] may nevertheless prove helpful. Still, it remains to be seen to which extent the mechanism of charge push-out is already built into today's organic solar cells, considering also that the CT-state energy should not be raised above the energy of a Frenkel exciton.

The link between driving-force polarity and molecular orientation and intermixing suggests morphological boundary conditions for efficient charge splitting. As a rule, there is a 2:1 trade-off between charge push-out forces versus photovoltaic gap, with operation just above an isopolar point providing an energetic compromise. We note, however, that this compromise only accounts for the structural factors that feature in the open-circuit voltage. An object of further study is hence to understand how the complex energy landscape for CT states that is suggested by calculations on interfaces with realistic patterning impacts dynamic factors that determine the steady-state charge density. Either way, the sensitivity of charge push-out forces to the degree of nanoscale surface roughness and molecular orientation as well as the implied trade-offs for cell energetics further illustrate why material choice and processing are such a formidable challenge for device fabrication.

AUTHOR INFORMATION

Corresponding Authors

*carl.poelking@mpip-mainz.mpg.de

DOI: 10.1021/jacs.5b02130
J. Am. Chem. Soc. 2015, 137, 6320−6326

*denis.andrienko@mpip-mainz.mpg.de

Notes

The authors declare no competing financial interest.

■ ACKNOWLEDGMENTS

We are grateful for financial support from the BMBF project MEDOS (FKZ 03EK3503B). We thank Aoife Fogarty, Patrick Gemünden, Jens Wehner and Anton Melnyk for critical reading of the manuscript.

■ REFERENCES

(1) Eftaiha, A. F.; Sun, J.-P.; Hill, I. G.; Welch, G. C. *J. Mater. Chem. A* **2014**, *2*, 1201.
(2) Sonar, P.; Fong Lim, J. P.; Chan, K. L. *Energy Environ. Sci.* **2011**, *4*, 1558.
(3) Boudreault, P.-L. T.; Najari, A.; Leclerc, M. *Chem. Mater.* **2011**, *23*, 456−469.
(4) Rao, A.; Wilson, M. W. B.; Hodgkiss, J. M.; Albert-Seifried, S.; Bässler, H.; Friend, R. H. *J. Am. Chem. Soc.* **2010**, *132*, 12698−12703.
(5) Yost, S. R.; Lee, J.; Wilson, M. W. B.; Wu, T.; McMahon, D. P.; Parkhurst, R. R.; Thompson, N. J.; Congreve, D. N.; Rao, A.; Johnson, K.; Sfeir, M. Y.; Bawendi, M. G.; Swager, T. M.; Friend, R. H.; Baldo, M. A.; Van Voorhis, T. *Nat. Chem.* **2014**, *6*, 492−497.
(6) Cnops, K., Rand, B. P., Cheyns, D., Verreet, B., Empl, M. A., Heremans, P. *Nat. Commun.*. **2014**5.
(7) Perez, M. D.; Borek, C.; Forrest, S. R.; Thompson, M. E. *J. Am. Chem. Soc.* **2009**, *131*, 9281−9286.
(8) Hoke, E. T.; Vandewal, K.; Bartelt, J. A.; Mateker, W. R.; Douglas, J. D.; Noriega, R.; Graham, K. R.; Fréchet, J. M. J.; Salleo, A.; McGehee, M. D. *Adv. Energy Mater.* **2013**, *3*, 220−230.
(9) Jeon, S. O.; Yook, K. S.; Chin, B. D.; Park, Y. S.; Lee, J. Y. *Sol. Energy Mater. Sol. Cells* **2010**, *94*, 1389−1392.
(10) Chen, H.-Y.; Hou, J.; Zhang, S.; Liang, Y.; Yang, G.; Yang, Y.; Yu, L.; Wu, Y.; Li, G. *Nat. Photonics* **2009**, *3*, 649−653.
(11) Poelking, C.; Tietze, C.; Elschner, M.; Olthof, S.; Hertel, D.; Baumeier, B.; Meerholz, K.; Würthner, F.; Leo, K.; Andrienko, D. *Nat. Mater.* **2015**, *14*, 434−439.
(12) D'Avino, G.; Mothy, S.; Muccioli, L.; Zannoni, C.; Wang, L.; Cornil, J.; Beljonne, D.; Castet, F. *J. Phys. Chem. C* **2013**, *117*, 12981−12990.
(13) Idé, J.; Méreau, R.; Ducasse, L. R.; Castet, F.; Bock, H.; Olivier, Y.; Cornil, J.; Beljonne, D.; D'Avino, G.; Roscioni, O. M.; Muccioli, L.; Zannoni, C. *J. Am. Chem. Soc.* **2014**, *136*, 2911−2920.
(14) Vandewal, K.; Albrecht, S.; Hoke, E. T.; Graham, K. R.; Widmer, J.; Douglas, J. D.; Schubert, M.; Mateker, W. R.; Bloking, J. T.; Burkhard, G. F.; Sellinger, A.; Fréchet, J. M. J.; Amassian, A.; Riede, M. K.; McGehee, M. D.; Neher, D.; Salleo, A. *Nat. Mater.* **2013**, *13*, 63−68.
(15) Provencher, F.; Bérubé, N.; Parker, A. W.; Greetham, G. M.; Towrie, M.; Hellmann, C.; Côté, M.; Stingelin, N.; Silva, C.; Hayes, S. C. *Nat. Commun.* **2014**, *5*, 1−11.
(16) Gregg, B. A. *J. Phys. Chem. Lett.* **2011**, *2*, 3013−3015.
(17) Caruso, D.; Troisi, A. *Proc. Natl. Acad. Sci. U.S.A.* **2012**, *109*, 13498−13502.
(18) Yost, S. R.; Van Voorhis, T. *J. Phys. Chem. C* **2013**, *117*, 5617−5625.
(19) Vandewal, K.; Tvingstedt, K.; Gadisa, A.; Inganäs, O.; Manca, J. V. *Nat. Mater.* **2009**, *8*, 904−909.
(20) Bakulin, A. A.; Rao, A.; Pavelyev, V. G.; Loosdrecht, P. H. M. v.; Pshenichnikov, M. S.; Niedzialek, D.; Cornil, J.; Beljonne, D.; Friend, R. H. *Science* **2012**, *335*, 1340−1344.
(21) McMahon, D. P.; Cheung, D. L.; Troisi, A. *J. Phys. Chem. Lett.* **2011**, *2*, 2737−2741.
(22) Gelinas, S.; Rao, A.; Kumar, A.; Smith, S. L.; Chin, A. W.; Clark, J.; van der Poll, T. S.; Bazan, G. C.; Friend, R. H. *Science* **2014**, *343*, 512−516.
(23) Thole, B. *Chem. Phys.* **1981**, *59*, 341−350.
(24) van Duijnen, P. T.; Swart, M. *J. Phys. Chem. A* **1998**, *102*, 2399−2407.
(25) Ren, P.; Ponder, J. W. *J. Phys. Chem. B* **2003**, *107*, 5933−5947.
(26) Stone, A. J. *J. Chem. Theory Comput.* **2005**, *1*, 1128−1132.
(27) Stone, A. J. *The Theory of intermolecular forces*; Clarendon Press: Oxford, 1997.
(28) Rühle, V.; Lukyanov, A.; May, F.; Schrader, M.; Vehoff, T.; Kirkpatrick, J.; Baumeier, B.; Andrienko, D. *J. Chem. Theory Comput.* **2011**, *7*, 3335−3345.
(29) May, F., Baumeier, B., Lennartz, C., Andrienko, D. *Phys. Rev. Lett.* **2012***109*.
(30) Linares, M.; Beljonne, D.; Cornil, J.; Lancaster, K.; Brédas, J.-L.; Verlaak, S.; Mityashin, A.; Heremans, P.; Fuchs, A.; Lennartz, C.; Idé, J.; Méreau, R.; Aurel, P.; Ducasse, L.; Castet, F. *J. Phys. Chem. C* **2010**, *114*, 3215−3224.
(31) Beljonne, D.; Cornil, J.; Muccioli, L.; Zannoni, C.; Brédas, J.-L.; Castet, F. *Chem. Mater.* **2011**, *23*, 591−609.
(32) Yost, S. R.; Wang, L.-P.; Van Voorhis, T. *J. Phys. Chem. C* **2011**, *115*, 14431−14436.
(33) Idé, J.; Mothy, S.; Savoyant, A.; Fritsch, A.; Aurel, P.; Méreau, R.; Ducasse, L.; Cornil, J.; Beljonne, D.; Castet, F. *Int. J. Quantum Chem.* **2013**, *113*, 580−584.
(34) Smith, E. R. *Proc. R. Soc. London, Ser. A* **1981**, *375*, 475−505.
(35) Westacott, P.; Tumbleston, J. R.; Shoaee, S.; Fearn, S.; Bannock, J. H.; Gilchrist, J. B.; Heutz, S.; deMello, J.; Heeney, M.; Ade, H.; Durrant, J.; McPhail, D. S.; Stingelin, N. *Energy Environ. Sci.* **2013**, *6*, 2756.
(36) Jamieson, F. C.; Domingo, E. B.; McCarthy-Ward, T.; Heeney, M.; Stingelin, N.; Durrant, J. R. *Chemical Science* **2012**, *3*, 485.
(37) A uniaxial thin-film symmetry (implying nematic order) with a coherence length far larger than the film thickness is already sufficient to foster long-range quadrupolar fields. This ordering is typically realized for polycrystalline materials, where each crystallite adopts a preferential out-of-plane (edge-on, tip-on, etc.) orientation on the substrate, whereas the in-plane orientations differ. Next to direct experimental evidence,[44] the presence of long-range ordering has also been verified through the comparison of calculated and measured ionization energies.[11]
(38) Burke, T. M.; McGehee, M. D. *Adv. Mater.* **2014**, *26*, 1923−1928.
(39) Tan, Z.-K.; Johnson, K.; Vaynzof, Y.; Bakulin, A. A.; Chua, L.-L.; Ho, P. K. H.; Friend, R. H. *Adv. Mater.* **2013**, *25*, 4131−4138.
(40) As a further downside of small atomistic models with imposed thermal disorder, finite-size-induced fluctuations of layer dipoles and quadrupoles limit a meaningful comparison of donor and acceptor energy levels to the vicinity of the interface (as depicted in Figure 2a).
(41) Note that the lattice description employs a damped intrapair charge−charge interaction (whose magnitude is overestimated due to the coarse-grained description) that recovers a typical electrostatic (i.e., first-order) electron−hole attraction energy of −1.6 eV, as for example seen in C_{60}:D5M.
(42) In the case of C_{60}:D5M the in-plane CT states correspond to a tip-on pair with a larger separation between hole and electron, leading to a reduced electronic coupling.
(43) Smith, S. L.; Chin, A. W. *Phys. Chem. Chem. Phys.* **2014**, *16*, 20305−20309.
(44) Elschner, C.; Schrader, M.; Fitzner, R.; Levin, A. A.; Bauerle, P.; Andrienko, D.; Leo, K.; Riede, M. *RSC Adv.* **2013**, *3*, 12117−12123.

DOI: 10.1021/jacs.5b02130
J. Am. Chem. Soc. 2015, 137, 6320−6326